Journal of Electronic Materials (2023) 52:251–257
https://doi.org/10.1007/s11664-022-09977-x

ORIGINAL RESEARCH ARTICLE

Effect of Thickness on Morphology, Structural, and Optical Properties of Nb-Doped β-Ga_2O_3 Films Prepared by RF Magnetron Sputtering

Ruidong Li[1,2] · Jinxiang Deng[1] · Peng Xie[3] · Qing Zhang[1] · Xue Meng[1] · Juxin Luo[1] · Guisheng Wang[1] · Qianqian Yang[1] · Hongli Gao[1]

Received: 13 May 2022 / Accepted: 16 September 2022 / Published online: 20 October 2022

Abstract

Here, niobium-doped monoclinic gallium oxide thin films of different thicknesses were deposited on p-Si (100) and quartz substrates by radio-frequency magnetron sputtering. All films were annealed in argon ambient. The crystal structure and surface morphology of the films were researched using x-ray diffraction and scanning electron microscopy. Then, their crystallite size was evaluated via the Debye–Scherrer formula. The results demonstrated that the films had a good crystal structure and a flat surface when the thickness was around 300 nm. The films' optical properties were also investigated, and the results showed that all of the films' transmittance is above 80% to ultraviolet–visible light whose wavelength is above 350 nm. Meanwhile, the films' optical band gap decreased as their thickness increased. The Urbach energy of all films was calculated by the Urbach rule, and the results indicated that the best crystal quality occurred when the thickness was around 300 nm. The films' electrical characteristics showed that the current was larger when the thickness was around 300 nm and that the contact between the Au electrode and films was Ohmic contact, independent of the film thickness and test conditions. These findings will provide useful information for the practical application of Nb-doped β-Ga_2O_3 thin films.

Keywords Thickness · Nb-doped β-Ga_2O_3 film · morphology · structure · optical properties · electrical characterization

Introduction

As a third-generation inorganic semiconductor, monoclinic gallium oxide (β-Ga_2O_3) shows promise for use in high-power electronics[1] and deep ultraviolet (UV) photodetectors[2–5] because of its ultrawide band gap in the range of 4.8–4.9 eV and the corresponding expected breakdown field, which can reach approximately 8 MV/cm^3. Although Ga_2O_3-based devices have attracted much attention in recent years, explorations of Ga_2O_3 date back several decades. However, earlier applications primarily focused on its basic physical properties and chemical synthesis.[6–10] From the 1990s to the 2010s, significant breakthroughs were made in the successful growth of large, high-quality bulk and thin-film crystals. Several methods used to grow β-Ga_2O_3 thin films have been developed, such as the sol–gel method,[5,11] molecular beam epitaxy,[2] the electron-beam evaporation method,[12] radio frequency (RF) magnetron sputtering,[13] and the metal organic chemical vapor deposition (MOCVD) method.[14] Of these, RF magnetron sputtering is simple in operation, good in film forming, and stable in performance. Additionally, it is suitable for use with semiconductor materials. In recent years, β-Ga_2O_3 has attracted much attention as a promising candidate for fabricating solar-blind photodetectors because of its intrinsic solar-blind band-gap of 4.9 eV, large absorption coefficient, and high chemical and thermal stability. However, the application of pure Ga_2O_3 is limited because of its poor thermal and electrical conductivity. Many researchers have attempted to improve the properties of Ga_2O_3 thin films through doping technology. Until now, several experiments and theoretical have been conducted to study the properties of β-Ga_2O_3 films incorporated with various impurities.[14–18] Of these impurities, niobium (Nb) is considered to be the best candidate for use

✉ Jinxiang Deng
jdeng@bjut.edu.cn

[1] Faculty of Science, Beijing University of Technology, Beijing 100124, China

[2] Department of Basic Courses, Institute of Disaster Prevention, Sanhe 065201, Hebei, China

[3] Institute of Urban Safety and Environmental Science, Beijing Academy of Science and Technology (Beijing Municipal Institute of Labour Protection), Beijing 100054, China

as an *n*-type dopant because Nb's atomic radius is very close to that of the Ga atom. The ionic radii of Nb^{5+} is almost the same as that of Ga^{3+}. The influence of Nb doping concentration and annealing atmosphere on the properties of Nb-doped β-Ga_2O_3 thin films have been investigated in others work.[19,20] The film thickness can also affect the properties of different kinds of thin films.[21,22] However, as far as we know, few scholars have touched upon the properties of Nb-doped β-Ga_2O_3 films prepared with different thickness. So we emphasize the real necessity of exploring the properties of Nb-doped β-Ga_2O_3 films prepared with different thickness.

The quality of films which are thinner or thicker is not sufficient. Therefore, in this study, Nb-doped β-Ga_2O_3 thin films of different thicknesses (223 nm—629 nm) were deposited using RF magnetron sputtering technology. The films' crystal structure and surface morphology were investigated, and their optical absorption and transmission spectra were also measured to study their optical properties. The study findings may be useful to researchers studying photodetectors based on β-Ga_2O_3.

Experimental

Here, Nb-doped β-Ga_2O_3 films with different thicknesses were directly deposited on p-Si (100) and quartz substrates by employing RF magnetron sputtering under Argon (Ar) ambient, with Ga_2O_3 (purity: 99.99%) and Nb_2O_5 (purity: 99.99%) targets. Before the sputtering, methylbenzene, acetone, and ethyl alcohol, in sequence, were used to clean the substrates for 15 min; an ultrasonic cleaner was used to remove organic contaminants. After that, the substrates were cleaned with deionized water and dried in N_2 gas.

Before the samples were deposited, the quartz and p-Si substrates were fixed on the platform in the vacuum chamber. The targets were pure Ga_2O_3 and Nb_2O_5. The distance between the targets and substrates was approximately 30 cm. The deposition chamber was evacuated to a pressure of ~ 10^{-4} Pa. Then, high-purity Ar (80 sccm) was introduced using mass flow controllers, and we used a throttle valve to keep the working pressure in the chamber at 1 Pa. The sputtering power of Nb_2O_5 and Ga_2O_3 were 40 and 80 W, respectively. The substrates were covered by a dam board before the film deposition. When the substrates reached the set temperature (100℃), the targets were presputtered for 10 min before formal sputtering was conducted to remove the surface impurities. Then, the dam board was removed, and the films were deposited. In order to make the films more uniform, the substrates were rotated at 15 rpm. Different Nb-doped β-Ga_2O_3 thin films were prepared for 3, 4, 5, 6, and 7 h at 100℃. All films were annealed for 2 h at 1173 K in Ar ambient.

The samples' surface morphology and crystal structure were characterized using a Hitachi S-4800 field emission scanning electron microscope and a Bruker D8 Advance x-ray diffraction (XRD) instrument equipped with Cu-Kα (λ = 1.5406 Å) radiation. Additionally, an ultraviolet (UV)–visible spectrophotometer (Shimadzu-3600) with a wavelength between 200 and 800 nm was used to analyze the films' optical properties. The samples' current–voltage (I–V) characteristics were measured via a Keithley 4200-SCS semiconductor characterization system at room temperature.

Results and Discussion

Figure 1a displays the scanning electron microscopy (SEM) image of the film that was prepared for 5 h. It can be seen that the sample had good contact with the p-Si substrate and that the interface was clear. From the cross section, we can clearly see the interface between the sample and the substrate and the film thickness was approximately 381 nm. If the interface between samples and substrate is not clear, it will cause some measuring error. Therefore, it is important to prepare the substrate before deposition. We measured the thicknesses of all the films, and the values are shown in Table I.

Figure 1b, c, and d illustrates the surface morphology of the films prepared for 5, 6, and 7 h, respectively. It can be seen that all film surfaces showed granular features. However, Fig. 1b shows that the surface of the 5-h film was more uniform and compact. As the sample thickness increased, the grain size gradually decreased. There were signs of cracking on the surfaces of the 458- and 629-nm films, demonstrating that the quality of the films deteriorated as the thickness increased.

Figure 2 shows the XRD patterns of all Nb-doped β-Ga_2O_3 films. It can be seen that peaks appeared around 22°, 30°, 33°, 38°, and 44°, corresponding to the (201), (110), (–111), (402), and (202) planes, respectively, of the Ga_2O_3 monoclinic phase. This demonstrated that β-Ga_2O_3 was formed. Figure 3a displays the peak position and intensity, and Fig. 3b shows the full width at half maximum (FWHM) and crystallite size of the (201) peak. It is worth mentioning that the intensity of the film with a thickness of 291 nm is stronger than that of 223 nm. However, the change of the diffraction peak intensities is not obvious.

As seen in Fig. 3a, the intensity of the (201) peak is the largest when the thickness of the film is about 300 nm. As shown in Fig. 3b, the full width at half maximum (FWHM) is the smallest when the thickness of the film is about 300 nm. Figure 3a and b indicates that the crystal quality of the films is the best when the thickness was 300 nm. The crystallite size (*D*) was calculated through the Debye–Scherrer formula:

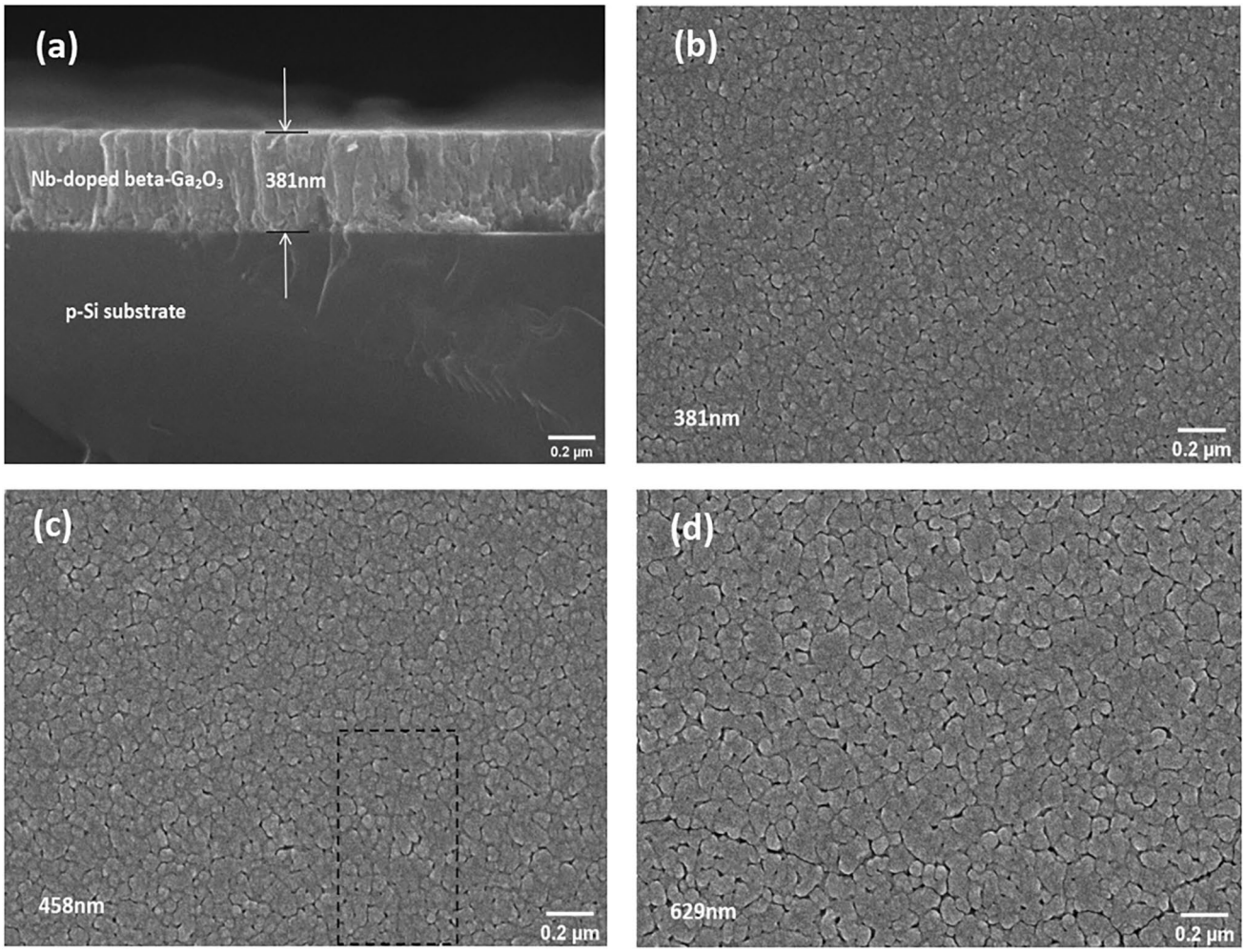

Fig. 1 SEM images of the Nb-doped β-Ga_2O_3 films: (a) cross section; (b)–(d) morphology and surface morphology.

Table I Thickness of the Nb-doped β-Ga_2O_3 films

Deposition time (hours)	3	4	5	6	7
Thickness (nm)	~223	~291	~381	~458	~629

$$D = \frac{0.9\lambda}{\beta \cos\theta},$$

where β is the width of the (201) peak at half maximum in radians, θ is the Bragg diffraction angle, and λ is the wavelength of the x-ray radiation. As shown in Fig. 3b, the crystallite size was larger when the film thickness was 300 nm, and the film quality was good. The results obtained from the FWHM and Debye–Scherrer formula agreed well with the SEM results.

To investigate the optical properties of the Nb-doped β-Ga_2O_3 thin films as the thickness increased, the optical absorption and transmission spectra of the films with

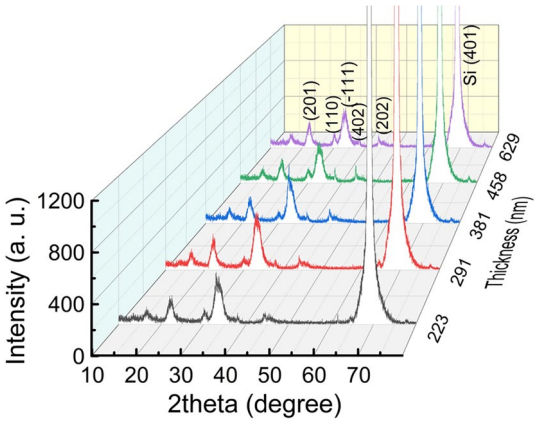

Fig. 2 XRD patterns of the Nb-doped β-Ga_2O_3 films with different thickness.

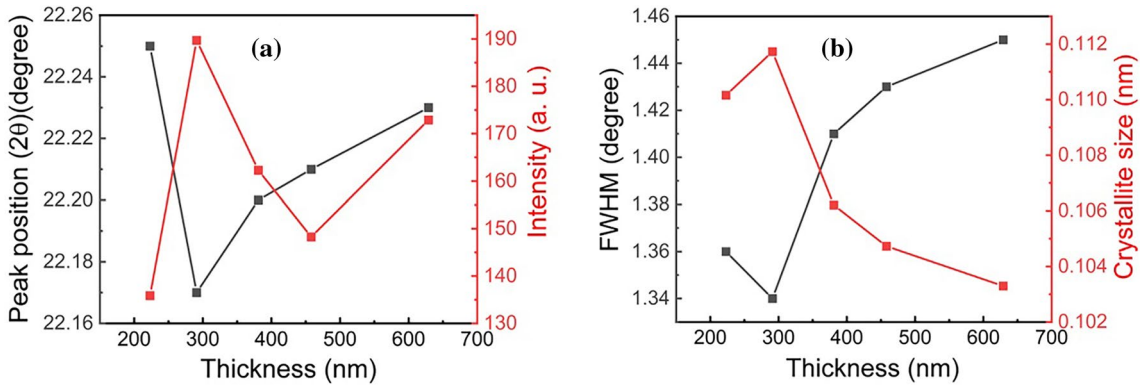

Fig. 3 XRD variation of (a) peak position and intensity; (b) FWHM and crystallite size.

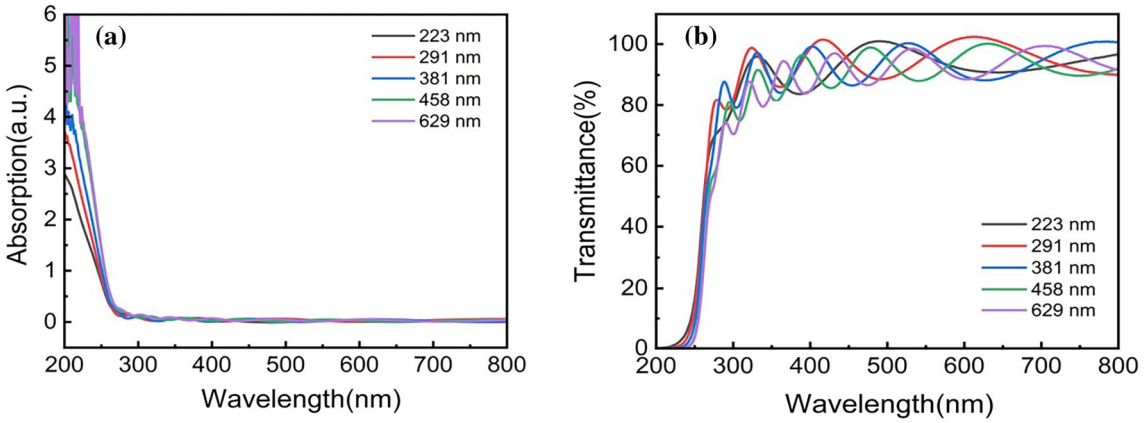

Fig. 4 Absorption spectra (a) and transmission spectra (b) of the Nb-doped β-Ga_2O_3 films with different thickness.

different thickness in the wavelength region 200 to 800 nm were measured, as shown in Fig. 4a and b. As shown in Fig. 4a, the samples had a high absorption value; the absorption edge showed a slight redshift. As shown in Fig. 4b, the transmittance of all samples is above 80% to UV–visible light with a wavelength above 350 nm. The optical band gap is usually a crucial optical parameter for photoelectrical devices. Here, the films' optical band gap was calculated using the Tauc equation[23]:

$$\alpha h\nu = A(h\nu - E_g)^{1/2},$$

where α is the absorption coefficient calculated using the relationship $\alpha = (\ln 1/T)/d$ from the transmission spectrum, where T is the transmittance, and d is the samples' thickness. Moreover, A is a constant, h is the Planck constant, ν is the frequency of incident photons in Hz, and E_g is the value of the optical band gap between the valence and conduction bands.

The films' optical band gaps were determined by the linear extrapolation of $(\alpha h\nu)^2$ against the $h\nu$ plot.[24] Figure 5

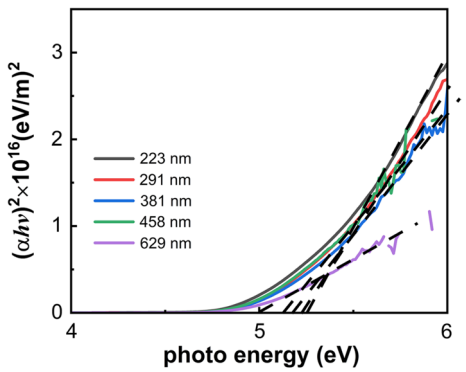

Fig. 5 Plot of $(\alpha h\nu)^2$ versus $h\nu$ of the Nb-doped β-Ga_2O_3 films with different thickness.

exhibits the typical variations of $(\alpha h\nu)^2$ versus $h\nu$ for the films of different thicknesses. A band gap value for this system was given as the intercept of the photon energy axis and linear line. Figure 6 illustrates the variation tendency

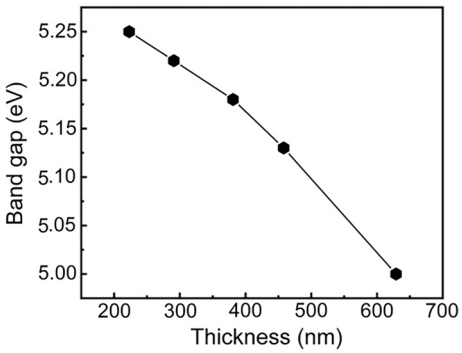

Fig. 6 Dependence of optical band gap on thickness of Nb-doped β-Ga_2O_3 films.

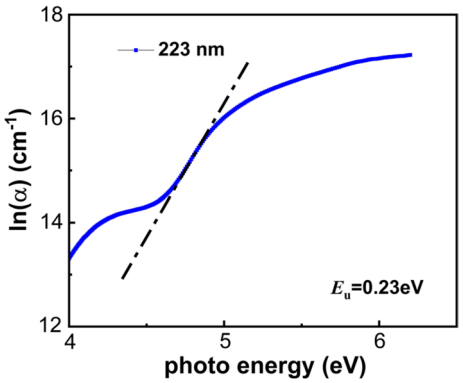

Fig. 7 The Urbach plot for the film with 223 nm.

of the optical band gap with the film thickness, showing that the optical band gap showed a slight redshift as the film thickness increased. Generally, different factors, such as grain size, carrier concentration, and deviation from the film stoichiometry, can cause a decrease of in the optical band gap.[25] Optical band gap values are higher when film thickness is lower due to the amorphous states.[26,27] A decrease in the optical band gap with an increase in thickness is usually caused by a shift in energy between the valence and conduction bands resulting from some effect, such as electron impurity.[28] A detailed analysis is needed to bring out the effect of each of these parameters on the value of band gap energy.

In this study, to check the films' crystal quality, the Urbach band tail was also measured for the five samples. Various factors, such as carrier–phonon interaction, carrier–impurity interaction, and structure disorder, can cause Urbach band tail changes in semiconductors.[29] Here, the Urbach energy (E_u) for the films was determined by the empirical Urbach rule[30] as follows[31]:

$$\alpha = \alpha_0 \exp\frac{h\nu - E_0}{E_u} = \alpha_0 \exp\frac{h\nu}{E_u}\left(h\nu < E_0\right)$$

where $h\nu$ is the photon energy, E_0 is the optical band gap, α_0 is a constant, and E_u is the Urbach energy. The E_u value provided more details about the samples' optical behavior. It was evaluated by fitting the absorption coefficient as a function of photon energy near the fundamental absorption edge.[32,33] Figure 7 shows the typical variations of ln(α) versus $h\nu$ for the 223-nm sample. The E_u value was obtained as the inverse slope of the straight line, representing ln(α) versus the photon energy. It was 0.22 eV when the film thickness was 223 nm. The values of all samples were calculated via the same method (Table II). Figure 8 shows the relationship between the E_u values and sample thickness. Generally, the E_u increased as the structural order increased.[34,35] Table II and Fig. 8 demonstrate that the structural order of

Table II Values of E_u at different thickness

Thickness (nm)	223	291	381	458	629
E_u (eV)	0.22	0.17	0.20	0.22	0.23

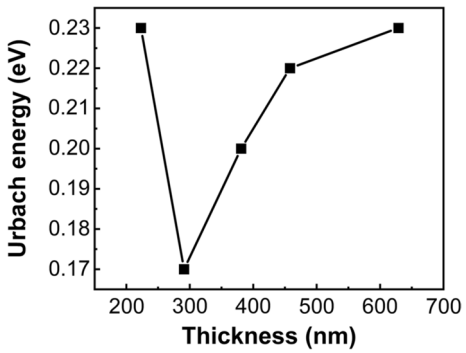

Fig. 8 Dependence of Urbach energy on thickness of Nb-doped β-Ga_2O_3 films.

the films first decreased and then increased when the film thickness was over 300 nm, consistent with the SEM images (Fig. 1) and XRD pattern (Fig. 2). This indicated that the system quality was highest when the film thickness was around 300 nm.

The films' electrical characteristics were also studied. Figure 9a shows the device structure, and Fig. 9b–d illustrates the current–voltage curves for this system. It can be seen that the Au electrode was in good contact with the samples and that Ohmic contact was formed between the electrode and Nb-doped β-Ga_2O_3 thin films, independent of the film thickness and test conditions. These findings will be useful for future work.

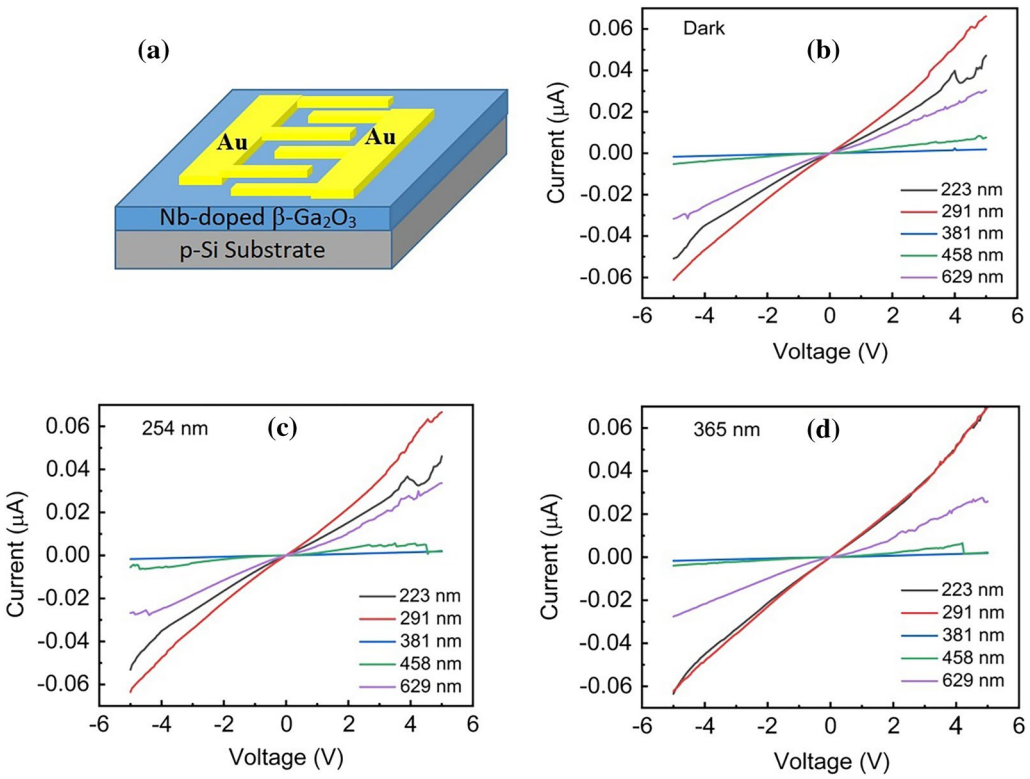

Fig. 9 Current–voltage curves of the Nb-doped β-Ga_2O_3 films: (a) the structure of device; (b)—(d) *I–V* curves of devices.

Conclusion

Nb-doped β-Ga_2O_3 thin films with different thicknesses were grown by RF magnetron sputtering technology. The dependence of the morphological and structural properties of Nb-doped β-Ga_2O_3 films on their thickness was investigated. Besides, we carried out an in-depth analysis of the influence of thickness on the optical and electrical properties of the films. The film had good flatness and crystal quality when the thickness was around 300 nm. The average transmittance of the Nb-doped β-Ga_2O_3 films in the visible region was above 80%, and the optical band gap decreased as the thickness increased. The films had a minimum defect density when the thickness was 291 nm. The contact between the samples and the Au electrode was Ohmic contact and was not influenced by the external environment. This research will aid in the practical application of Nb-doped β-Ga_2O_3 thin films.

Acknowledgments This work is supported by the Beijing Nova Program (Grant No. Z211100002121079), the Funding for the Development Project of Beijing Municipal Education Commission of Science and Technology (Grant No. KZ201410005008), and the Natural Science Foundation of Beijing City, China (Grant Nos. 4192016, 4102014).

Conflict of interest This manuscript has not been published elsewhere and is not under consideration by another journal. All authors of this manuscript have no potential conflict of interest including any financial or non-financial, or personal with each other.

References

1. M.H. Wong, K. Sasaki, A. Kuramata, S. Yamakoshi, and M. Higashiwaki, Field-Plated Ga_2O_3 MOSFETs With a Breakdown Voltage of Over 750 V. *IEEE Electron. Device Lett.* 37, 212–215 (2016).
2. A.S. Pratiyush, S. Krishnamoorthy, S.V. Solanke, Z.B. Xia, R. Muralidharan, S. Rajan, and D.N. Nath, High Responsivity in Molecular Beam Epitaxy Grown β-Ga_2O_3 Metal Semiconductor Metal Solar Blind Deep-UV Photodetector. *Appl. Phys. Lett.* 110, 221107 (2017).
3. R. Suzuki, S. Nakagomi, and Y. Kokubun, Solar-Blind Photodiodes Composed of a Au Schottky Contact and a β-Ga_2O_3 Single Crystal with a High Resistivity Cap Layer. *Appl. Phys. Lett.* 98, 1114 (2011).
4. T. Oshima, T. Okuno, N. Arai, N. Suzuki, S. Ohira, and S. Fujita, Vertical Solar-Blind Deep-Ultraviolet Schottky Photodetectors Based on β-Ga_2O_3 Substrates. *Appl. Phys. Express* 1, 011202 (2008).
5. Y. Kokubun, K. Miura, F. Endo, and S. Nakagomi, Sol–gel Prepared β-Ga_2O_3 Thin Films for Ultraviolet Photodetectors. *Appl. Phys. Lett.* 90, 031912 (2007).
6. L. Havestadt, and R. Fricke, Dielectric Behavior of Oxide Hydrates. *Z. Anorg. Allg. Chem.* 188, 357–395 (1930).
7. A. Brukl, and G. Ortner, The Oxides of Gallium. *Z. Anorg. Allg. Chem.* 203, 23–25 (1931).

8. G. Centola, Thermal Decomposition of Some Gallium Salts and the Structure of the Resulting Oxides. *IX Congreso Internacional de Química Pura y Aplicada* 3, 230–238 (1934).
9. M.L. Guernsey, The Spectrum of Gallium Oxide. *Phys. Rev.* 46, 114–116 (1934).
10. A.W. Laubengayer, and H.R. Engle, The Sesquioxide and Hydroxides of Gallium. *J. Amer. Chem. Soc.* 61, 1210–1214 (1939).
11. L.B. Cheah, R.A.M. Osman, and P. Poopalan, Ga_2O_3 Thin Films by Sol-Gel Method and its Optical Properties. *AIP Conf. Proc.* 2203, 020028 (2020).
12. S.J. Li, C. Yang, J. Zhang, L.P. Dong, C.L. Cai, H.F. Liang, and W.G. Liu, Tunable Optical Properties of Amorphous-Like Ga_2O_3 Thin Films Deposited by Electron-Beam Evaporation with Varying Oxygen Partial Pressures. *Nanomaterials* 10, 1760 (2020).
13. R.D. Li, J.X. Deng, L. Kong, J.H. Meng, J.X. Luo, Q. Zhang, H.L. Gao, Q.Q. Yang, G.S. Wang, and X.L. Wang, Infuence of Substrate Temperature on Structure and Properties of Nb-Doped β-Ga_2O_3 Films. *Jour. Elec. Mate.* 51, 2390–2395 (2022).
14. W. Mi, X.J. Du, C.N. Luan, H.D. Xiao, and J. Ma, Electrical and Optical Characterizations of β-Ga_2O_3: Sn Films Deposited on MgO (110) Substrate by MOCVD. *RSC Adv.* 4, 30579 (2014).
15. Z.P. Wu, G.X. Bai, Q.R. Hu, D.Y. Guo, C.L. Sun, L.Y. Ji, M. Lei, L.H. Li, P.G. Li, J.H. Hao, and W.H. Tang, Effects of Dopant Concentration on Structural and Near-Infrared Luminescence of Nd^{3+}-Doped Beta-Ga_2O_3 Thin Films. *Appl. Phys. Lett.* 106, 171910 (2015).
16. A.A. Dakhel, Structural, Optical, and Opto-dielectric Properties of W-Doped Ga_2O_3 Thin Films. *J. Mater. Sci.* 47, 3034–3039 (2012).
17. X.H. Wang, F.B. Zhang, K. Saito, T. Tanaka, M. Nishio, and Q.X. Guo, Electrical Properties and Emission Mechanisms of Zn-Doped β-Ga_2O_3 Films. *J. Phys. Chem. Solid.* 75, 1201–1204 (2014).
18. H. Peelaers, and C.G. Van de Walle, Doping of Ga_2O_3 with Transition Metals. *Phys. Rev. B* 94, 195203 (2016).
19. H. Zhang, J.X. Deng, Z.W. Pan, Z.Y. Bai, L. Kong, and J.Y. Wang, Structural and Optical Properties of Nb-Doped β-Ga_2O_3 Thin Films Deposited by RF Magnetron Sputtering. *Vacuum* 146, 93–96 (2017).
20. H. Zhang, J.X. Deng, L. Kong, Z.W. Pan, Z.Y. Bai, and J.Y. Wang, Effect of Annealing Atmosphere on the Structural and Optical Properties of the Nb-Doped β-Ga_2O_3 Films. *Micro&Nano. Lett.* 14, 62–65 (2019).
21. X. Ji, Y.M. Mi, Z. Yan, and C.M. Zhang, Influence of Thickness on the Structural, Optical and Electrical Properties of $CuInSe_2$ Absorbing Layer for Photovoltaic Applications. *Optoelectron. Adv. Mater.* 6, 483–486 (2012).
22. Y.H. Ding, R.S. Cai, Q.T. Du, Y.Q. Wang, Y.Z. Chen, and J.R. Sun, Microstructure Evolution of Bi04Ca06MnO3 Epitaxial Films with Different Thickness. *J. Cryst. Growth* 317, 115–118 (2011).
23. H. Shen, X. Zhao, L. Duan, R. Liu, H. Li, and B. Wang, Efect of NaZn/Nai Ratio on Structural, Optical, and Electrical Properties of Na-Doped ZnO Thin Films. *J. Appl. Phys.* 121, 155303 (2017).
24. G.C. Xie, L. Fang, L.P. Peng, G.B. Liu, H.B. Ruan, F. Wu, and C.Y. Kong, Effect of In-Doping on the Optical Constants of ZnO Thin Films. *Phys. Procedia* 32, 651 (2012).
25. K.G. Saw, N.M. Aznan, F.K. Yam, S.S. Ng, and S.Y. Pung, New Insights on the Burstein-Moss Shift and Band Gap Narrowing in Indium-Doped Zinc Oxide thin Films. *PLoS ONE* 10, 0141180 (2015).
26. E. Vega, S.B. Isukapati, and T.N. Oder, Microstructure and Optical Properties of Sputter-Deposited Ga_2O_3 Films. *J. Vacuum Sci. Technol. A* 39, 033412 (2021).
27. S.S. Kumar, E.J. Rubio, M.N. Alam, G. Martinez, S. Manandhar, V. Shutthanandan, S. Thevuthasan, and C.V. Ramana, Structure, Morphology, and Optical Properties of Amorphous and Nanocrystalline Gallium Oxide Thin Films. *J. Phys. Chem. C* 117, 4194 (2013).
28. I. Hamberg, and C.G. Granvist, Evaporated Sn-Doped In_2O_3 Films: Basic Optical Properties and Applications to Energy-Efficient Windows. *J. Appl. Phys.* 60, 123 (1986).
29. H.S. Nalwa ed., *Handbook of Organic Conductive Molecules and Polymers*. (New York: Wiley, 1997).
30. F. Urbach, The Long-Wavelength Edge of Photographic Sensitivity and of the Electronic Absorption of Solids. *Phys. Rev.* 92, 1324 (1953).
31. C.H. Grein, and S. John, Temperature Dependence of the Urbach Optical Absorption Edge: A Theory of Multiple Phonon Absorption and Emission Sidebands. *Phys. Rev. B* 39, 1140 (1989).
32. J.A. Banday, F.A. Mir, M.A. Qurishi, S. Koul, and T.K. Razdan, Isolation, Structural, Spectral, and Thermal Studies of Imperatorin Micro-crystals from Prangos Pabularia. *J. Therm. Anal. Calorim.* 112, 1165 (2013).
33. Y.R. Sharma, and O.P. Vig, *Elementary Organic Spectroscopy*, 3rd ed., (New Delhi: S. Chand and Company Ltd., 1999).
34. J. Xie, B. Li, Y.J. Li, P. Yan, L.J. Feng, Y.P. Cai, J.G. Zheng, J.Q. Zhang, W. Li, L.L. Wu, Z. Lei, and G.G. Zeng, Study of ZnS Thin Films Prepared by RF Magnetron Sputtering Technique. *Acta. Phys. Sini.* 59, 5749–5754 (2010).
35. F. Liu, C. Ding, Y.H. Zhang, T.S. Ripolles, T. Kamisaka, T. Toyoda, S. Hayase, T. Minemoto, K. Yoshino, S.Y. Dai, M. Yanagida, and H. Noguchi, Q, Shen, Colloidal Synthesis of Air-Stable Alloyed $CsSn_{1-x}Pb_xI_3$ Perovskite Nanocrystals for Use in Solar Cells. *J. Am. Chem. Soc.* 139, 16708–16719 (2017).